PAPER • OPEN ACCESS

In-depth photoluminescence analysis of Cu_2GeS_3 microcrystals under pulsed and continuous-wave excitation

IOP Publishing J. Phys. Energy 7 (2025) 035003 https://doi.org/10.1088/2515-7655/adc836

Journal of Physics: Energy

OPEN ACCESS

RECEIVED
23 January 2025

REVISED
18 March 2025

ACCEPTED FOR PUBLICATION
1 April 2025

PUBLISHED
10 April 2025

PAPER

In-depth photoluminescence analysis of Cu_2GeS_3 microcrystals under pulsed and continuous-wave excitation

Jüri Krustok*, Joel Kokla, Reelika Kaupmees, Maarja Grossberg-Kuusk and Marit Kauk-Kuusik

Department of Materials and Environmental Technology, Tallinn University of Technology, Ehitajate tee 5, 19086 Tallinn, Estonia
* Author to whom any correspondence should be addressed.

E-mail: Juri.Krustok@taltech.ee

Keywords: photoluminescence, excitons, trions, CW laser, pulsed laser, DA pairs, band-to-band recombination

Supplementary material for this article is available online

Abstract

In this study, an in-depth photoluminescence (PL) analysis of Cu_2GeS_3 microcrystals under pulsed and continuous-wave (CW) excitation is performed to explore the optical properties and defect structure of this promising novel absorber material for indoor photovoltaics. A rich low-temperature ($T = 8$ K) PL spectra with multiple peaks was detected by both excitation sources and analyzed in detail. The edge emission, including free and bound excitons as well as unique trion emission at 1.575 eV, which becomes dominant under the pulsed laser excitation, enabling clear detection of its properties. At higher temperatures also band-to-band emission is observed under the CW excitation, and the donor-acceptor pair recombination with its phonon replica is dominating the PL spectra revealing a shallow donor defect with an ionization energy of 35 meV and a slightly deep acceptor defect with an ionization energy of 119 meV. In addition, from the temperature dependencies of the PL peaks, an extremely weak electron-phonon coupling in CGS was found. The observed edge emission and detected rather shallow defects emphasize the high crystalline quality and the suitability of Cu_2GeS_3 for photovoltaic applications.

1. Introduction

Advanced materials for photovoltaic (PV) applications are being investigated as a result of the global need for sustainable energy solutions. Among these, indoor photovoltaics (IPVs) have attracted a lot of interest since they make it possible to harvest energy from artificial light sources, providing a viable way to power low-energy electronics and Internet of Things devices [1]. Choosing appropriate absorber materials that can efficiently transform low-intensity light into electricity is a crucial part of creating effective IPV systems.

Because of their readily available raw materials, tunable optical characteristics, and low toxicity, copper-based ternary and quaternary chalcogenides, such $Cu(In,Ga)Se_2$ and $Cu_2ZnSn(S,Se)_4$, have demonstrated significant potential in traditional PV applications. Cu_2GeS_3 (CGS), a novel absorber material with unique properties that make it ideal for indoor PV applications, has recently surfaced. This material is better suited for absorbing the spectrum of indoor light sources like LEDs and fluorescent lamps since it has a direct bandgap around 1.5–1.6 eV [2–4]. Its high absorption coefficient, *p*-type conductivity, and outstanding stability further demonstrate its potential as a long-lasting and effective absorber material. It is demonstrated that, despite the detection of orthorhombic and cubic phases, CGS preferentially exhibits a monoclinic crystal structure (space group *Cc*) [5–7]. The investigation of Cu_2GeS_3 for IPV applications is still in its early stages, despite these benefits. There is a substantial information gap about its behavior and optimization under interior lighting conditions because the majority of previous research has concentrated on its synthesis, structural characterisation, and performance in outdoor PV systems. The highest efficiency of CGS/CdS solar cell is reported to be only 2.67% [8]. However, as demonstrated in [9], CdS is not the ideal buffer layer for CGS absorbers; instead, $Cd_{0.5}Zn_{0.5}S$ must be used for improved band alignment. Further enhancement of the power conversion efficiency requires also a thorough comprehension of the fundamental properties of CGS.

To describe the optical characteristics of semiconductors, photoluminescence (PL) spectroscopy is frequently employed. Free and bound exciton peaks, along with broader donor-acceptor pair (DAP) bands, have been observed in the first low temperature PL measurements of CGS under continuous-wave (CW) excitation [5]. All of these peaks displayed thermal activation energies below 23 meV, which is extremely low. At $T = 5$ K, the free exciton (FE) peak had a maximum at 1.5935 eV. Recently, a room-temperature PL of Cu_2GeS_3 microcrystals grown in molten LiI salt were analyzed [3]. There were two types of crystals found: A and B. The PL spectra of type B crystals were composed of four distinct PL bands, whereas type A crystals displayed a PL band at 1.57 eV and a weak band at about 1.68 eV. Two band gaps were discovered: $E_{G1} = 1.564$ eV and $E_{G2} = 1.675$ eV. They are linked to the spin-orbit split V2 valence band and the upmost valence band V1, respectively. Spin-orbit splitting energy was determined to be 0.11 eV. The connection between the V1 and V2 valence bands to the same acceptor level at a depth of 90 meV was shown. To gain a better understanding of the excitonic emission and recombination processes involving deeper defect levels, more research on the PL characteristics of CGS is required. It is well known that using pulsed or CW lasers for excitation results in significant differences in PL characteristics. The binary compound Sb_2Se_3 is a nice example, where FE and biexcitons were revealed by utilizing a pulsed UV laser ($\lambda = 266$ nm, pulse width 0.6 ns) to exploit a high PL excitation density [9]. No biexcitons were found when CW laser was used for excitation [10]. It was demonstrated that the multiexciton population scales nonlinearly with power; therefore, under the identical experimental conditions, pulsed excitation should generate almost 150 times as many multiexcitons as CW excitation [11].

In this study, we provide a comprehensive PL examination of Cu_2GeS_3 microcrystals as an IPV absorber material by using both CW and pulsed lasers for excitation. The results of this study help to develop next-generation IPV technologies and facilitate the shift to more sustainable and energy-efficient methods of powering electronic devices indoors.

2. Experimental details

The ternary Cu_2GeS_3 microcrystallite powder was produced by combining commercially available Cu powder (99.999%, Alfa Aesar), Ge powder (99.999%, Alfa Aesar), and S powder (99.999%, Alfa Aesar). The precursor materials were weighed into graphitized quartz ampoule inside a glove box. The ampoule was used to prevent any mutual reaction between Ge and quartz. The precursor mixture was degassed, the ampoule was sealed, and then heated at a rate of approximately 0.5 °C min^{-1} from room temperature to 700 °C over 20 h. The ampoule was subsequently maintained at 700 °C for two weeks, and then cooled in air.

The surface morphology and shape of the produced microcrystals were examined using the Zeiss MERLIN high-resolution scanning electron microscope (SEM). Our microcrystals were, on average, around 20 μm in size (figure 1). Energy dispersive x-ray spectroscopy (EDX) was used to analyze the bulk composition of the generated powder crystals using the Bruker EDX-XFlash 6/30 detector and an accelerating voltage of 20 kV (the measurement error is around 0.5 at%). EDX analysis of the microcrystals revealed an average composition of 35.2 at% of Cu, 16.2 at% of Ge, and 48.6 at% of S, i.e. it was slightly Cu-rich ($Cu_{2.2}GeS_3$). The CGS microcrystals primarily have a monoclinic crystal structure, as we previously reported in our recent paper [3]. The XRD pattern of 2 different measurements and the reference pattern of monoclinic Cu_2GeS_3 (ICDD 01-088-0827) were presented in figure S1.

The Raman measurements were carried out using a Horiba LabRAM HR800 Micro-Raman system with a cooled multichannel CCD detection system in the backscattering configuration and a spectral resolution better than 1 cm^{-1}. For excitation, a second harmonics of Nd:YAG laser with a wavelength of 532 nm was employed. The diameter of the laser spot was roughly 3 μm and the power density was as high as 30 kW cm^{-2}. As seen in figure 2, the peaks in the deconvoluted Raman spectra of Cu_2GeS_3 microcrystals were resolved using a Lorentzian function. All of the Raman peaks belong to Cu_2GeS_3 and have been identified in numerous papers before [3, 8, 12–14].

Cu_2GeS_3 microcrystals were positioned on the cold finger of the closed-cycle helium cryostat (Janis CCS-150) in order to perform temperature-dependent PL measurements. After that, the temperature was lowered to 8 K. A LakeShore Model 335 temperature controller was used to control the temperature up to 300 K. A second harmonics of Cobolt 08-DPL Nd:YAG laser operating at 532 nm was used to provide CW PL excitation. CW laser maximum average power was $P_{max} = 37$ mW. Neutral density filters were used to change the incident laser beam's power density from 0.04 to 0.3 Wcm^{-2}. A second harmonics of pulsed Q-switched CryLaS FQSS266-Q2 Nd:YAG laser (532 nm) with a maximum average power $P_{max} = 7.5$ mW, peak energy 1.1 μJ, and peak width <1 ns at 10 kHz was employed as a pulsed excitation source. The pulsed laser intensity was also decreased using the same neutral density filters. For both lasers, the laser spot size was approximately 1 mm. The PL signal was acquired using optical fiber, then sent to the same Horiba LabRAM

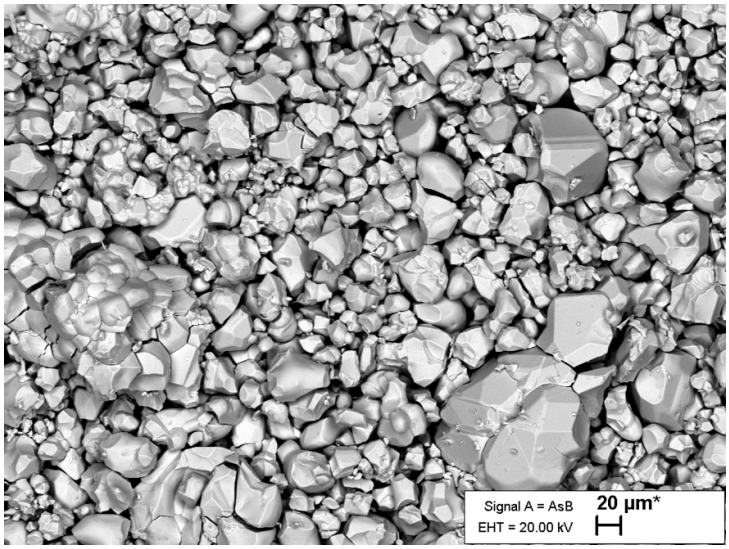

Figure 1. SEM image of Cu_2GeS_3 microcrystals. Additionally, larger sintered microcrystals are also visible.

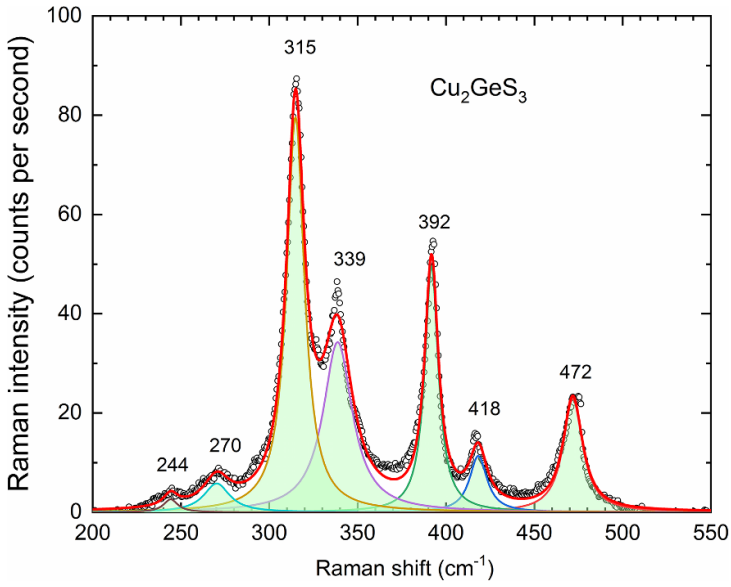

Figure 2. Typical Raman spectrum of Cu_2GeS_3 microcrystals. Peak fitting results using a Lorentzian function are shown.

HR800 Micro-Raman system with a 600 lines per mm grating for recording using a cooled multichannel CCD detection system in the backscattering configuration.

3. Results and discussion

The PL spectra of CGS sample measured at $T = 8$ K using CW and pulsed lasers are presented in figure 3. There are a number of PL peaks shared by both excitation sources.

However, the T peak becomes dominant under pulsed excitation, while the DAP peak prevails under CW laser excitation. All PL spectra were fitted using an asymmetric hyperbolic secant (AHS) function:

$$I(E) = I_0 / \left[\exp\left(\left(E - E_M\right)/W_{HE}\right) + \exp\left(-\left(E - E_M\right)/W_{LE}\right)\right], \quad (1)$$

where W_{HE} and W_{LE} are related to the width of high and low energy sides of the PL band, respectively, while E_M is related to the peak position E_{max}. Example of this fitting is presented in figure 4. The AHS function was chosen because it gave the best fitting result. Peak parameters E_{max}, full width at half maximum (FWHM), and I_{max} were numerically calculated from the fitting function. There is an unexpected spectral region from

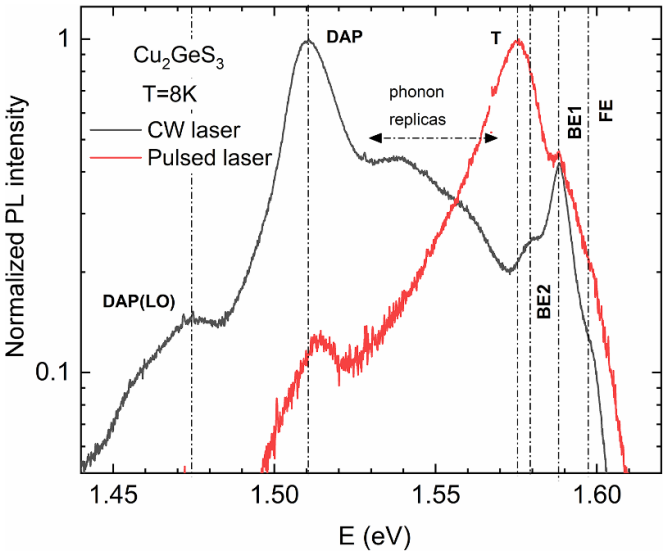

Figure 3. Normalized PL spectra of Cu_2GeS_3 microcrystals at T = 8 K measured with CW (black) and pulsed (red) laser excitation. Peak positions are marked as vertical lines.

1.53 to 1.57 eV marked as phonon replicas in figures 3 and 4(a). Similar region was discovered also by Aihara *et al* [12]. In this area, the PL spectra lack a distinct structure with distinct PL peaks and are probably a combination of different phonon replicas of edge emission peaks FE, BE1, and BE2, as was first proposed by Aihara *et al* [12]. However, further research is necessary to determine the true origin of this spectral region. Although we fitted two broad peaks to this region in figure 4(a), it is unlikely that this fitting is completely correct. It seems that different phonons are involved, and therefore we have such a unexpected spectral region. Although LO-phonons frequently play a larger role in the electron-phonon interaction for PL peaks, lower energy phonons can also be seen on occasion [15].

Unfortunately, when measured with a pulsed laser, the intensity of the FE peak at $T = 8$ K was very weak; however, as the temperature increases, its presence will be more noticeable (see figure 7). As a result, we excluded the FE peak from the fitting in figure 4(b).

Peak positions of all peaks at $T = 8$ K are presented in table 1.

The FE position is 1.599 eV, which is marginally higher than what was found in [12]. Additionally, two bound excitons, BE1 and BE2, are visible. The PL peak at 1.475 eV is most probably related to the first LO phonon replica of the DAP peak. Thus, the LO phonon energy in Cu_2GeS_3 is around 36–40 meV. This phonon replica's comparatively low intensity suggests that the electron-phonon interaction for DAP recombination is extremely weak.

Figure 5 presents the excitation power dependence of the PL spectra of CGS measured at $T = 8$ K using both lasers.

As the laser power increases, almost all PL peaks do not shift. On the other hand, the DAP peak clearly displays a blueshift of 3–4 meV for every decade increase of laser power. This emission peak behavior is typical of DAP recombination and results from the separation inhomogeneity (near and distant spacing) of DAP. As the laser excitation power increases, the PL of more distant DA pairs will be saturated, and more closely spaced pairs having a higher recombination probability are excited, which causes the band to blueshift [16]. Unfortunately, when measured with a pulsed laser, the peak position shift of the DAP peak is not as noticeable, as shown in figure 5. This peak's extremely low intensity and overlap with the T peak are partially to blame. For the excitonic region, we observed PL intensity saturation and even a decrease at higher CW laser powers, whereas under pulsed laser excitation, all peaks displayed a steady rise with increasing laser power. Consequently, we employed a lower laser power $P = 0.3\ P_{max}$ for temperature-dependent measurements using CW laser.

Generally, the excitation power dependence of the PL intensity serves as a reliable indicator of the characteristics of radiative recombination processes. In particular, the laser excitation power, P, exhibits a power law dependence on the integral PL intensity, Φ, as $\Phi \propto P^m$. When m is less than 1, it indicates a recombination path with defects, and when m is close to 1, it indicates an exciton-like transition. Trions, in which three particles are involved in the recombination process, should exhibit a $P^{1.5}$ dependence, meaning that the intensity should increase superlinearly with laser power, and P^2 dependence is expected for biexcitons [17, 18]. The dependence of integral intensity of PL bands on laser power is presented in figure 6.

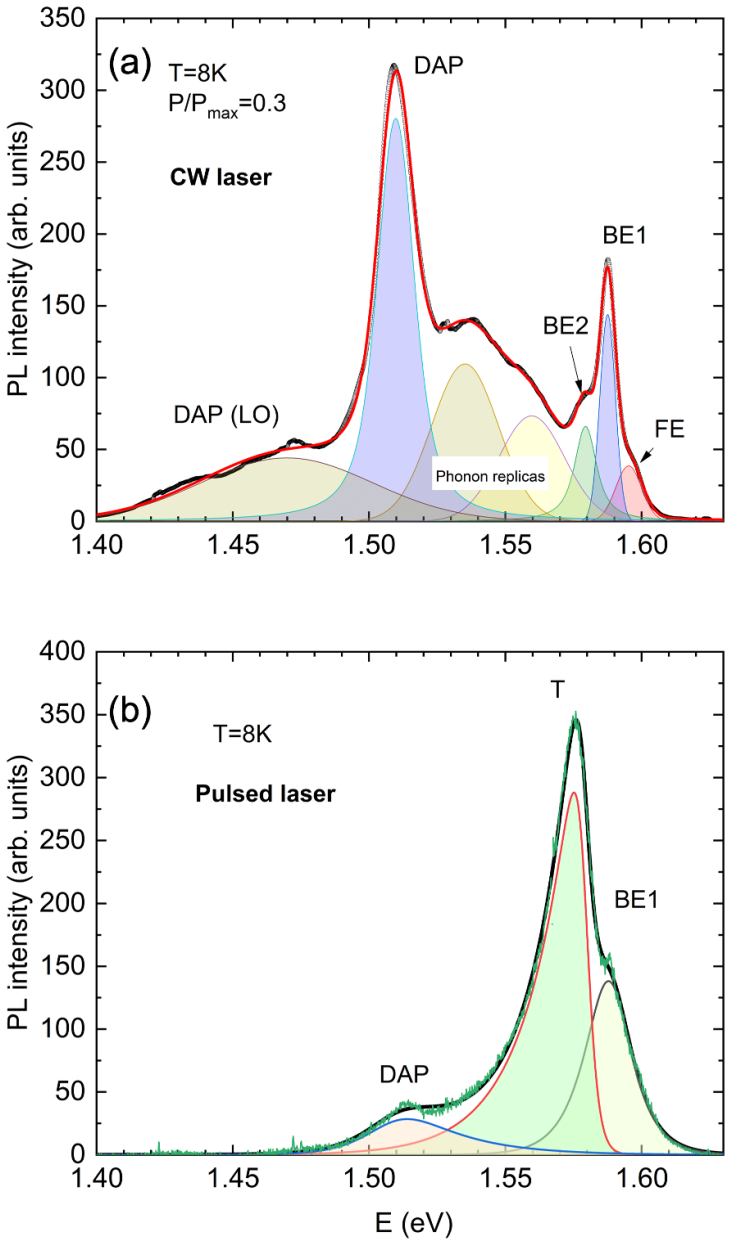

Figure 4. An illustration of fitting PL peaks with the AHS function for CW excitation (a) and pulsed excitation (b) at T = 8 K.

Table 1. Cu_2GeS_3 main PL peak positions at T = 8 K.

PL peak	E_{max} (eV)	Laser
FE	1.599	CW, pulsed
BE1	1.589	CW, pulsed
BE2	1.579	CW
T	1.575	Pulsed
DAP	1.511	CW, pulsed
DAP(LO)	1.475	CW

The DAP peak with $m = 0.86$ is clearly related to defects, and therefore the DAP model is applicable. The T peak with $m = 1.5$ indicates trion emission, while the BE1 peak is most likely associated with bound exciton emission. A trion is formed when either an electron or hole binds to an exciton. Compared to nanocrystals, quantum wells or monolayers, trion emission is less frequently seen in bulk crystals. Consequently, it is surprising that the formation of trions in our CGS microcrystals is encouraged by pulsed laser excitation with a pulse length of less than 1 ns. To the best of our knowledge, no papers have reported the detection of trion emission in single crystals. The shape of almost all PL peaks is fairly symmetrical,

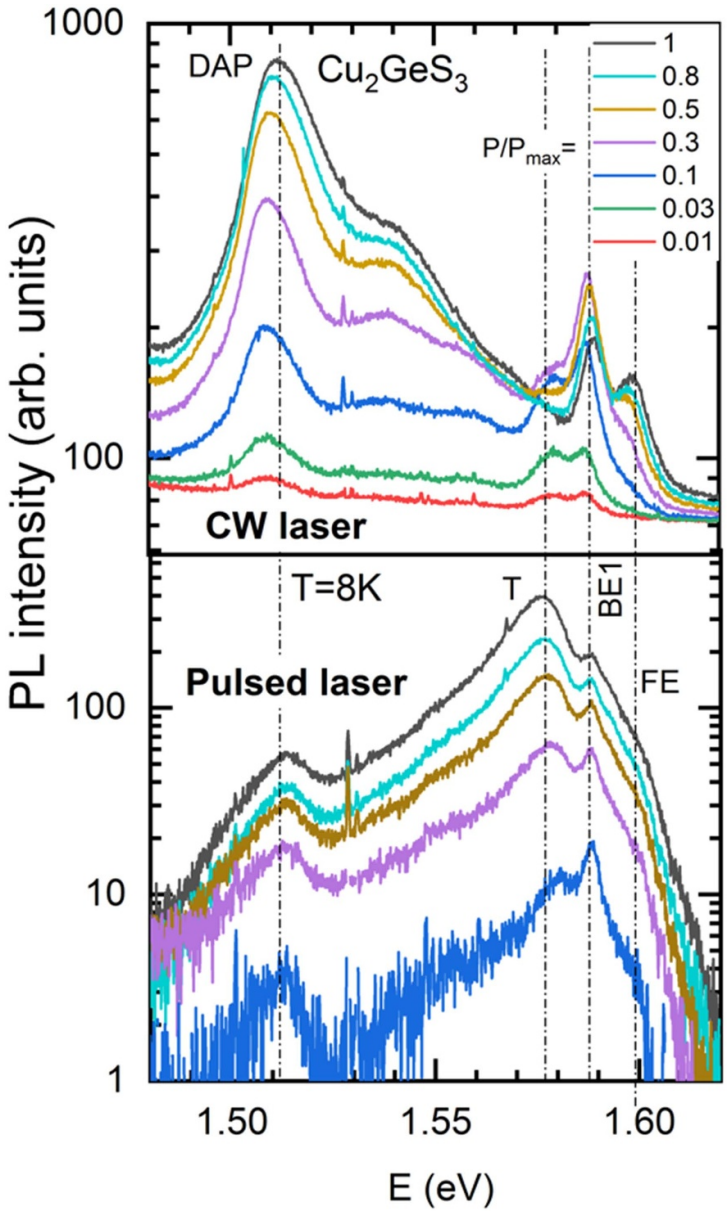

Figure 5. Excitation power dependencies of Cu_2GeS_3 microcrystals PL measured at $T = 8$ K using CW and pulsed lasers.

however as seen in figures 4(b) and 5, the trion peak T exhibits a pronounced asymmetry, with the high-energy slope being steeper than the low-energy one. There is an important difference between exciton and trion emission in different compounds. While only zero-momentum exciton states are coupled to light, radiative recombination of non-zero momentum trions is also allowed. This leads to an asymmetric broadening of the trion spectral peak and the redshift of the emitted light with increasing temperature. The trion spectral shape is therefore strongly affected by the trion momentum distribution and the momentum-dependent trion decay rate [19]. When trions decay radiatively, they release an electron. All trions can decay radiatively because the recoil electron removes all of the trion's momentum. This causes the trion PL peaks to have an asymmetric shape, with the low energy tail representing a Boltzmann distribution of trion kinetic energies. The thermal distribution and effective electron and hole masses are thus revealed by the low-energy tail. The low-energy tail widens with increasing temperature, and trions typically have this asymmetric structure in different materials [20, 21].

Next, under excitation of both lasers, the temperature dependence of Cu_2GeS_3 PL emission was measured, as illustrated in figure 7.

The PL peaks' thermal activation energies were derived from the Arrhenius plot (figure 8), where a theoretical expression for discrete energy levels was used to fit the dependence of ln Φ (T) versus $1000/T$ [22]:

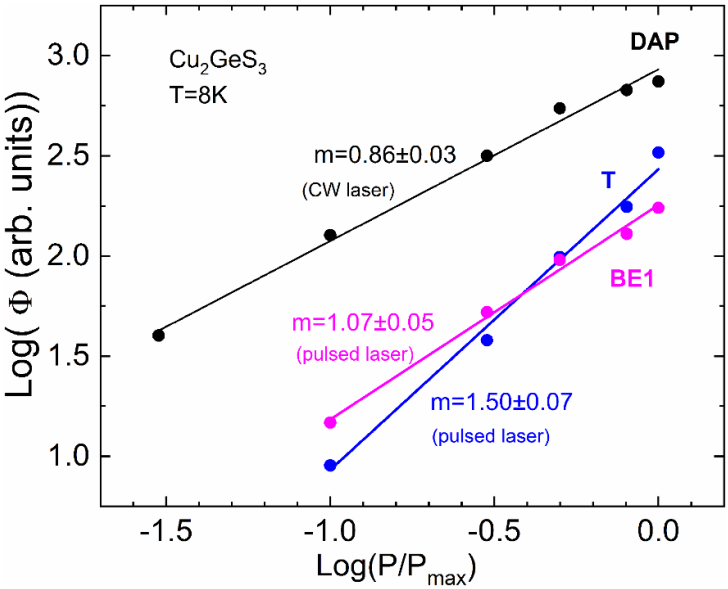

Figure 6. Integrated photoluminescence intensity of main PL bands as a function of the laser power plotted on a log–log scale. The lines are least squares fit to the data.

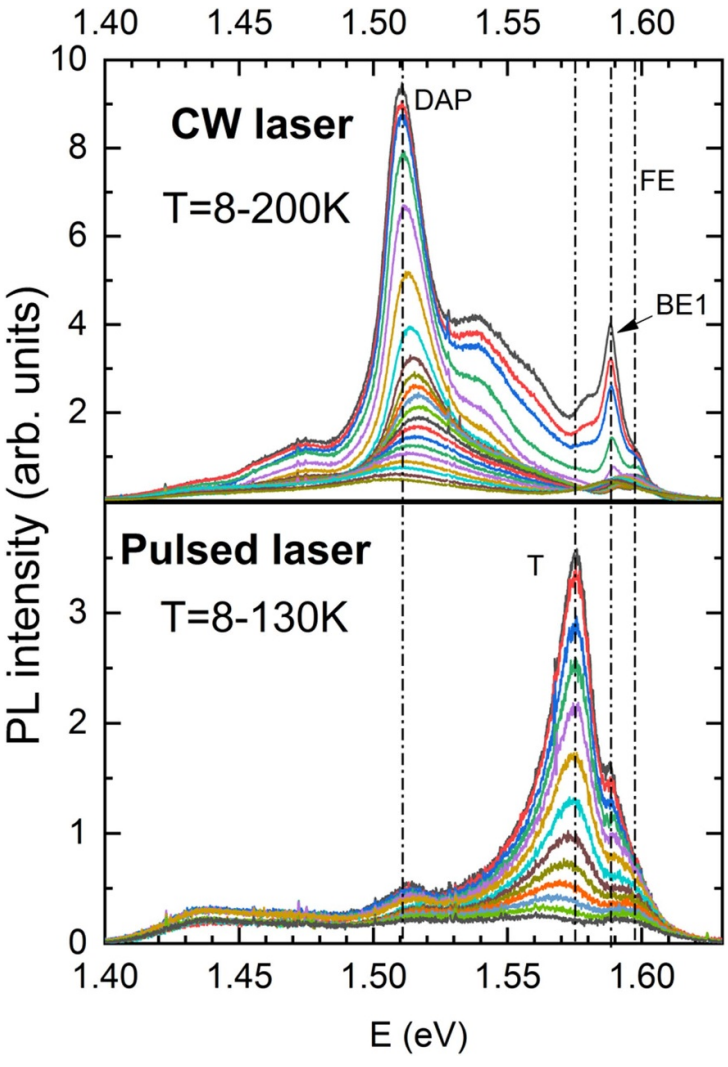

Figure 7. Temperature dependence of Cu_2GeS_3 microcrystals measured with CW and pulsed lasers.

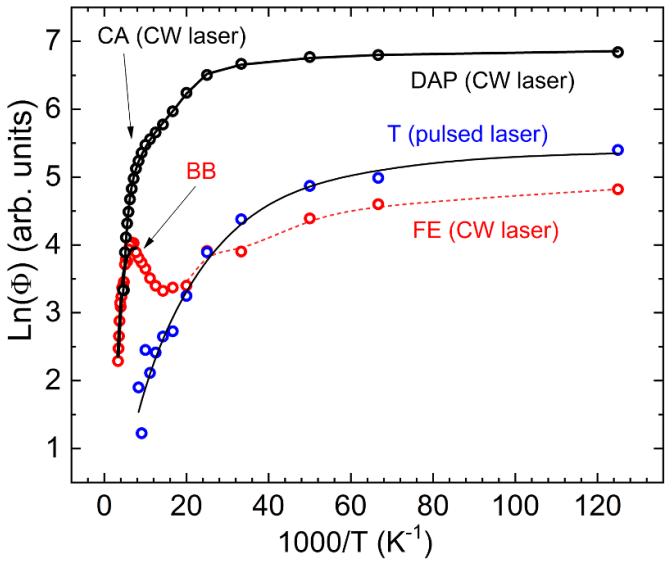

Figure 8. Arrhenius plots derived from the temperature dependence of PL spectra of Cu_2GeS_3. Solid lines are result of fitting with equation (2).

Table 2. Thermal quenching activation energies E_A for different PL peaks.

PL peak	BB	T	DAP	CA
E_A (meV)	100 ± 15	6 ± 3	35 ± 5	119 ± 17

$$\phi\,(T) = \phi_0 / \left[1 + A_1 T^{3/2} + A_2 T^{3/2} \exp\left(-E_A/kT\right)\right], \tag{2}$$

where Φ is an integrated intensity of the PL peak, A_1 and A_2 are the process rate parameters and E_A is the thermal activation energy.

The two-stage quenching of the DAP peak is evident. At approximately $T = 100$ K, the second recombination process begins to dominate with an activation energy $E_A = 119$ meV, whereas the lower temperature region displays an activation energy $E_A = 35$ meV. Assuming that the shallow donor level of DAP will be ionized at higher temperatures and that a straightforward conduction band to acceptor level (CA) recombination will begin to manifest, this behavior can be explained. FE emission exhibits very similar behavior, with FE recombination changing to band-to-band (BB) recombination at $T \approx 50$ K. The intensity of the BB peak increases as a result of the FE dissociating. The activation energy of the BB peak is $E_A = 100$ meV, and it is probably related to the activation of nonradiative recombination channels. The trion peak (T) shows a thermal activation energy $E_A = 6$ meV. This value is less than what is typically found in different compounds, mostly in 2D materials. Unfortunately, the fitting of the T peak quenching is far from being perfect. The integrated intensity values show quite a big scattering at higher temperatures. The R^2 value of this fitting was only 0.964, and therefore the activation energy for T peak is somewhat doubtful. Table 2 lists the thermal activation energies for four distinct recombinations.

It is highly likely that the ionization of the acceptor level is connected to the quenching of the CA recombination. This level's depth is then approximately 119 meV. The distance between the BB and CA peak positions allows us to estimate this depth as well. Figure 9 shows that the separation is approximately 81 meV. A very similar acceptor level (90 meV) was detected also in our previous paper [3]. Thus, considering potential errors, it is highly likely that we are dealing with the same acceptor level resulting from an intrinsic defect at a depth of about 90 meV.

Figure 9. Shows a temperature dependence of peak positions for different PL peaks. Experimental data points of several peaks at $T = 8$–300 K were fitted with O'Donnell's expression [23]:

$$E_{\max}\,(T) = E_{\max}\,(0) - S\langle E_{\rm ph}\rangle \left[\coth\left(\langle E_{\rm ph}\rangle / 2kT\right) - 1\right] \tag{3}$$

where $E_{\max}(0)$ is the peak position at $T = 0$ K, S is a dimensionless coupling constant and $<E_{\rm ph}>$ represents an average phonon energy. Fitting parameters are given in table 3.

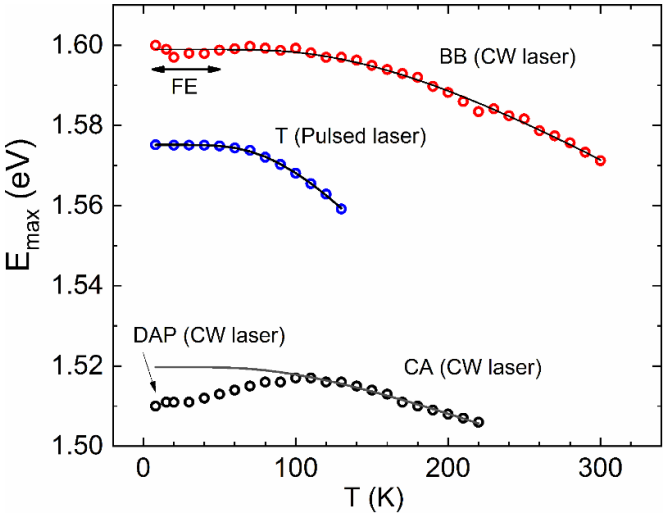

Figure 9. Peak positions of the PL bands as a function of temperature. Fitting with equation (3) results are given with solid lines.

Table 3. Fitting parameters obtained from the fitting with equation (3) for different PL peaks of Cu_2GeS_3 microcrystals.

PL peak	FE, BB	T	CA
E_{max} (0) (eV)	1.5989 ± 0.0002	1.5752 ± 0.0001	1.519 ± 0.001
S	1.42 ± 0.09	3.3 ± 0.1	0.9 ± 0.2
$<E_{ph}>$ (meV)	44 ± 2	29.0 ± 0.1	29 ± 8

The temperature dependence of the bandgap energy is largely represented by the shift of the FE and BB peaks. The phonon energy $<E_{ph}\geqslant 44$ meV is very close to the LO phonon energy estimated from the positions of DAP and DAP(LO) PL peaks. An indirect indication that lower-energy phonons are also included in the electron-phonon coupling of PL peaks is the 29 meV phonon energy displayed by the CA and T peaks. According to table S1, the phonon energies of about 40 and 29 meV correlate to Raman peaks 315 and 244 cm^{-1}, respectively. Compared to the FE (and BB) peaks, the trion peak T exhibits a redshift with increasing temperature that is significantly faster. It was shown in [21] that the emitted photon energy of trion E_T is given by

$$E_T = E_{T0} - \frac{m_X}{m_e} E_{TK} \tag{4}$$

where E_{T0} is the zero-momentum trion energy, m_X is the exciton mass, m_e is the effective electron mass, and E_{TK} is the trion kinetic energy. Increasing the temperature also increases the kinetic energy of trions, and this leads to the redshift, which is faster than the redshift of bandgap energy E_G determining the shift of E_{T0}.

As the temperature rises, the DAP band initially exhibits a blueshift. However, at around 100 K, when CA recombination begins to take over, it will redshift at a rate that is comparable to that of the BB peak. This is typical behavior for DAP recombination, where shallow donor defects will be ionized and the conduction band to acceptor recombination appears. The estimated depth of this donor level is around 10 meV; see figure 9.

Figure 10 shows the FWHM's temperature dependence for the main PL peaks. The temperature dependence of the FWHM for T peak was fitted using the relation proposed by Rudin and Reinecke [24] given as

$$\text{FWHM}\ (T) = W_0 + \beta T + W_1 / \left[\exp\left(\langle E_{ph}\rangle / kT\right) - 1\right] \tag{5}$$

where W_0 is the width at $T = 0$ K including also inhomogeneous broadening, β is a coefficient for the interaction of excitons with acoustic phonons and the last term represents the interaction with optical phonons, $<E_{ph}>$ is the phonon energy. The interaction with acoustic phonons was neglected because it is usually very small. The obtained phonon energy $<E_{ph}\geqslant 26$ meV is very similar to the value determined by the temperature dependence of the trion peak position E_{max} (see table 3). This provides further evidence that at least two phonons are involved in the radiative recombination in Cu_2GeS_3 microcrystals. The temperature dependence of half-width at half-maximum (HWHM) values for the T peak is displayed in the inset of

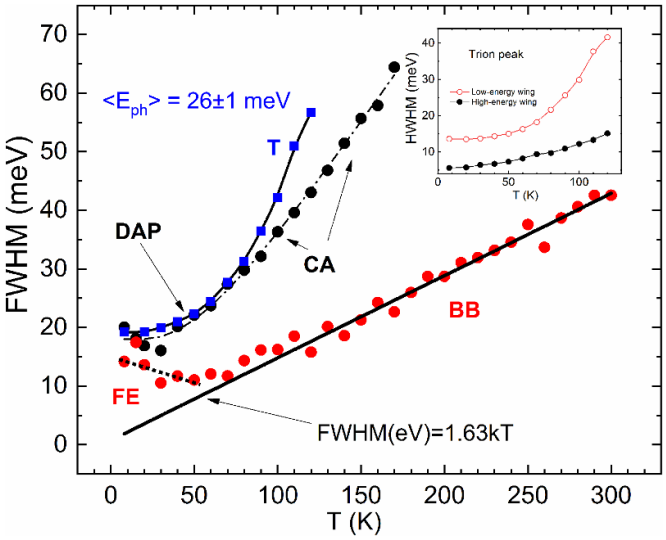

Figure 10. The FWHM's temperature dependence for the primary PL peaks. The trion peak's *HWHM* values are displayed in the inset. Fitting results are presented as continuous lines.

figure 10. This behavior—where the low-energy wing widens more quickly than the high-energy wing—was predicted theoretically and found experimentally in a variety of systems. It is attributed to the Boltzmann distribution of trions' kinetic energies [20, 21, 25, 26]. Due to the overlap of both peaks, the FWHM temperature dependencies of the DAP and CA recombinations was rather complex. Consequently, we skip a fitting for these peaks. The behavior of the FE and BB peaks was quite different. The FE recombination is transformed into BB recombination with a perfect linear increase of FWHM with temperature starting at $T = 50$–60 K. It is known that the shape of the BB emission in nearly perfect crystals can be calculated as

$$I(E) \propto \sqrt{(E - E_G)}\exp\left(-\frac{E}{kT}\right) \tag{6}$$

i.e. it is a combination of density of states function for carriers and a Boltzmann distribution function. The theoretical width of this emission band is FWHM $\approx 1.8kT$. In reality, the density of states function often deviates from the theoretical model, and the electron-phonon interaction along with defects contribute additional complexity to the shape of the BB peak and to the FWHM value. For example, in order to account for the experimentally measured shape of the high-energy wing, the carrier temperature $T_C > T$ is used in the Boltzmann distribution part of equation (6). Therefore, the $1.8kT$ dependence can be slightly different. In our case we have FWHM $\approx 1.63kT$, i.e. it is quite close to the theoretical value. The linear trend of FWHM provides evidence that the Boltzmann distribution function is primarily responsible for the widening of the BB band and suggests that the electron-phonon coupling in CGS must be extremely weak.

4. Conclusions

In conclusion, the PL spectra of Cu_2GeS_3 microcrystals measured at $T = 8$ K showed a variety of peaks under both CW and pulsed Nd:YAG laser excitation (532 nm), with the unique trion (T) peak at 1.575 eV dominating under pulsed excitation and the DAP peak at 1.511 eV prevailing under CW excitation. The FE position was 1.599 eV, and two bound excitons, BE1 and BE2, were at 1.589 and 1.579 eV, respectively. The spectra revealed interesting features such as phonon replicas in the region 1.53–1.57 eV, likely a mix of different phonon replicas, but further research is needed to fully understand their origin. The excitation power dependence of the PL spectra of CGS measured at T = 8 K with both lasers showed that the DAP peak exhibited a blueshift of 3–4 meV for every decade increase in laser power, consistent with DAP recombination. In contrast, the T peak displayed behavior typical of trion emission and the BE1 peak is associated with bound excitons.

The temperature dependence of the Cu_2GeS_3 PL emission revealed important insights into the thermal activation energies and recombination processes. The DAP peak undergoes two-stage quenching, with activation energies of 35 meV at lower temperatures and 119 meV at higher temperatures, indicating ionization of shallow donor levels and transition to conduction band to acceptor recombination. Similarly, the FE emission transition to BB recombination at around 50 K was detected. The trion peak exhibited a low

thermal activation energy of 6 meV, suggesting unique behavior compared to other materials. The temperature dependence of peak positions and widths was consistent with electron-phonon interactions, with the FE and BB peaks showing linear broadening, and the trion peak exhibiting a faster redshift than the redshift of bandgap energy E_G. These findings provide valuable understanding of the temperature-driven behavior of recombination processes in Cu_2GeS_3, particularly the weak electron-phonon coupling and the influence of phonons in the radiative recombination.

Data availability statement

All data that support the findings of this study are included within the article (and any supplementary files).

Acknowledgment

This work was supported by European Union through the European Regional Development Fund, Project TK210, by the Estonian Research Council Grant PRG1023 and the research was conducted using the NAMUR+ core facility funded by the Estonian Research Council (TT13).

Conflict of interest

The authors declare that they have no known competing financial interests or personal relationships that could have appeared to influence the work reported in this paper.

ORCID iDs

Jüri Krustok https://orcid.org/0000-0002-4671-2332
Joel Kokla https://orcid.org/0009-0003-9022-201X
Reelika Kaupmees https://orcid.org/0000-0002-1766-4837
Maarja Grossberg-Kuusk https://orcid.org/0000-0003-3357-189X
Marit Kauk-Kuusik https://orcid.org/0000-0003-0071-8568

References

[1] Srivishnu K S, Rajesh M N, Prasanthkumar S and Giribabu L 2023 Photovoltaics for indoor applications: progress, challenges and perspectives *Sol. Energy* **264** 112057
[2] Li X, Timmo K, Grossberg M, Pilvet M, Kaupmees R, Krustok J, Muska K, Mikli V and Kauk-Kuusik M 2022 Study of the structure and optoelectronic properties of $Cu_2Ge(Se_xS_{1-x})_3$ microcrystalline powders *Thin Solid Films* **742** 139053
[3] Krustok J, Kaupmees R, Kokla J and Kauk-Kuusik M 2024 Optical study of valence band splitting and resonant acceptor states in Cu_2GeS_3 microcrystals *Appl. Phys. Lett.* **125** 242111
[4] Chen Q, Maeda T and Wada T 2018 Optical properties and electronic structures of Cu_2SnS_3, Cu_2GeS_3, and their solid solution $Cu_2(Ge,Sn)S_3$ *Jpn. J. Appl. Phys.* **57** 08RC20
[5] Robert E V C, de Wild J, Colombara D and Dale P J 2016 Crystallographic and optoelectronic properties of the novel thin film absorber Cu_2GeS_3 *Thin Films for Solar and Energy Technology VIII* vol 9936, ed M J Heben and M M Al-Jassim p 993607
[6] Neumann H, Riede V, Sharif N, Sobotta H and Omar M S 1989 Infrared lattice vibrations and crystal structure of Cu_2GeS_3 *J. Mater. Sci. Lett.* **8** 1360–1
[7] Araki H, Yamano M, Nishida G, Takeuchi A, Aihara N and Tanaka K 2017 Synthesis and characterization of $Cu_2Sn_{1-x}Ge_xS_3$ *Phys. Status Solidi* C **14** 1600199
[8] Jin X, Zhang L, Jiang G, Liu W and Zhu C 2017 High open-circuit voltage of ternary Cu_2GeS_3 thin film solar cells from combustion synthesized Cu-Ge alloy *Sol. Energy Mater. Sol. Cells* **160** 319–27
[9] Krustok J, Kondrotas R, Nedzinskas R, Timmo K, Kaupmees R, Mikli V and Grossberg M 2021 Identification of excitons and biexcitons in Sb_2Se_3 under high photoluminescence excitation density *Adv. Opt. Mater.* **9** 2100107
[10] Kondrotas R, Nedzinskas R, Krustok J, Grossberg M, Talaikis M, Tumėnas S, Suchodolskis A, Žaltauskas R and Sereika R 2022 Photoreflectance and photoluminescence study of antimony selenide crystals *ACS Appl. Energy Mater.* **5** 14769–78
[11] Smyder J A, Amori A R, Odoi M Y, Stern H A, Peterson J J and Krauss T D 2014 The influence of continuous vs. pulsed laser excitation on single quantum dot photophysics *Phys. Chem. Chem. Phys.* **16** 25723–8
[12] Aihara N, Matsumoto Y and Tanaka K 2017 Photoluminescence characterization of Cu_2GeS_3 bulk crystals *Phys. Status Solidi* b **254** 1700118
[13] Matsumoto Y, Aihara N, Saito N and Tanaka K 2017 Growth of Cu_2GeS_3 bulk single crystals by chemical vapor transport with iodine *Mater. Lett.* **194** 16–19
[14] Kim Y and Choi I-H 2019 Pressure-dependent Raman spectra of Cu_2GeS_3 and Cu_2SnS_3 *J. Alloys Compd.* **770** 959–63
[15] Krustok J, Raudoja J and Jaaniso R 2006 Temperature dependence of very deep emission from an exciton bound to an isoelectronic defect in polycrystalline $CuInS_2$ *Appl. Phys. Lett.* **89** 2–5
[16] Williams F 1968 Donor—acceptor pairs in semiconductors *Phys. Status Solidi* b **25** 493–512
[17] Schmidt T, Lischka K and Zulehner W 1992 Excitation-power dependence of the near-band-edge photoluminescence of semiconductors *Phys. Rev.* B **45** 8989–94
[18] Moon S, Thi Nguyen A, Cho J, Song J, Cho E, Lim S, Cho C-H and Kim D-W 2024 Enhanced trion emission from WS_2 monolayers directly exfoliated on Ag nanohole arrays *J. Alloys Compd.* **1002** 175241

[19] Scharf B, Van Tuan D, Žutić I and Dery H 2019 Dynamical screening in monolayer transition-metal dichalcogenides and its manifestations in the exciton spectrum *J. Phys.: Condens. Matter* **31** 203001
[20] Esser A, Runge E, Zimmermann R and Langbein W 2000 Electron and hole trions in wide GaAs quantum wells *Phys. Status Solidi* b **221** 281–6
[21] Christopher J W, Goldberg B B and Swan A K 2017 Long tailed trions in monolayer MoS_2: temperature dependent asymmetry and resulting red-shift of trion photoluminescence spectra *Sci. Rep.* **7** 14062
[22] Krustok J, Collan H and Hjelt K 1997 Does the low-temperature Arrhenius plot of the photoluminescence intensity in CdTe point towards an erroneous activation energy? *J. Appl. Phys.* **81** 1442–5
[23] O'Donnell K P and Chen X 1991 Temperature dependence of semiconductor band gaps *Appl. Phys. Lett.* **58** 2924–6
[24] Rudin S and Reinecke T L 1990 Temperature-dependent exciton linewidths in semiconductor quantum wells *Phys. Rev.* B **41** 3017–27
[25] Esser A, Runge E, Zimmermann R and Langbein W 2000 Trions in GaAs quantum wells: photoluminescence lineshape analysis *Phys. Status Solidi* a **178** 489–94
[26] Ross J S *et al* 2013 Electrical control of neutral and charged excitons in a monolayer semiconductor *Nat. Commun.* **4** 1474